J. Biophotonics **9**, No. 7, 709–714 (2016) / **DOI** 10.1002/jbio.201500283

Journal of BIOPHOTONICS

FULL ARTICLE

Multicolor multiphoton microscopy based on a nanosecond supercontinuum laser source

Claire Lefort[*, 1], *Rodney P. O'Connor*[1], *Véronique Blanquet*[1], *Laetitia Magnol*[1], *Hideaki Kano*[2], *Vincent Tombelaine*[3], *Philippe Lévêque*[1], *Vincent Couderc*[1], *and Philippe Leproux*[1, 3]

[1] Université de Limoges, CNRS UMR 7252, Labex "Sigma-Lim", INRA UMR 1061, F-87000 Limoges, France
[2] Institute of Applied Physics, University of Tsukuba, 1-1-1 Tennodai, Tsukuba, Ibaraki, 305-8573, Japan
[3] LEUKOS Innovative Optical Systems, 37 rue Henri Giffard, Z.I. Nord, 87280 Limoges, France

Received 23 October 2015, revised 19 December 2015, accepted 6 January 2016
Published online 15 February 2016

Key words: multiphoton microscopy, nonlinear imaging, nanosecond supercontinuum source, multicolor imaging

Multicolor multiphoton microscopy is experimentally demonstrated for the first time on a spectral bandwidth of excitation of 300 nm (full width half maximum) thanks to the implementation a nanosecond supercontinuum (SC) source compact and simple with a low repetition rate. The interest of such a wide spectral bandwidth, never demonstrated until now, is highlighted *in vivo*: images of glioma tumor cells stably expressing eGFP grafted on the brain of a mouse and its blood vessels network labelled with Texas Red® are obtained. These two fluorophores have a spectral bandwidth covering the whole 300 nm available. In parallel, a similar image quality is obtained on a sample of mouse muscle *in vitro* when excited with this nanosecond SC source or with a classical high rate, femtosecond and quasi monochromatic laser. This opens the way for (i) a simple and very complete biological characterization never performed to date with multiphoton processes, (ii) multiple means of contrast in nonlinear imaging allowed by the use of numerous fluorophores and (iii) other multiphoton processes like three-photon ones.

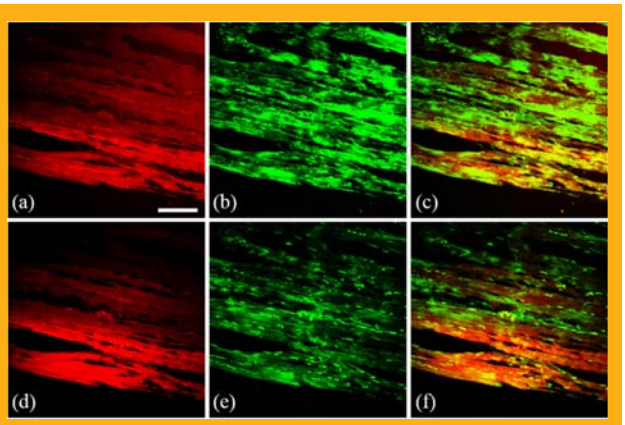

1. Introduction

Multiphoton microscopy (MPM) is a widespread technique for high resolution, three dimensional and deep imaging of living or excised tissues, involving nonlinear processes [1] such as two-photon fluorescence (TPF) and second harmonic generation (SHG) [2]. The TPF emission rate of a defined fluorophore depends on the parameters of the excitation laser [3–6]: pulse duration τ, repetition rate f

* Corresponding author: e-mail: claire.lefort@xlim.fr

and average power $\bar{P}$ and follows the law related to pulse peak power $\hat{P}$:

$$\Psi \propto \eta \hat{P} \propto \eta \frac{\bar{P}^2}{f\tau} \quad (1)$$

η being a constant value depending on the excitation wavelength, the two-photon cross section of the fluorophore and the characteristics of the objective. Considering Eq. (1), several combinations between $\bar{P}$, τ and f are likely to generate multiphoton processes.

Since many years, quasi-monochromatic MHz femtosecond lasers in the near infrared (NIR), and mainly titanium sapphire (Ti : Sa) sources, are primarily used for MPM [7]. These sources present several advantages: high repetition rate, low pulse energy, large spectral tunability and high average power. Other monochromatic sources have also been used marginally such as nanosecond [8], picosecond [4] and sub-picosecond lasers [9]. Different pulse lengths from 100 fs to 100 ps with a constant repetition rate allow to obtain similar multiphoton interactions [10–12] provided that average power is sufficient and respects Eq. (1).

Beyond the temporal aspect of the excitation source, its spectral properties have their own importance in MPM, and can lead to the definition of three criteria: (i) a spectral tunability allows to excite a large panel of exogenous or endogenous fluorophores; (ii) a broad spectrum has the potentiality to image several fluorophores simultaneously (multicolor MPM), even those with very distant two-photon absorption (TPA) spectra; (iii) a shaped spectrum allows to be adapted at best to the TPA spectrum of the fluorophore. Thus, ultrabroadband sources, named supercontinuum (SC), have found their place in MPM [13]. Such sources are typically based on the spectral broadening of femtosecond pulses in a photonic crystal fiber (PCF) associated with a prior or subsequent complex and expensive step of pulse shaping [14]. These high rate femtosecond sources having a spectral bandwidth of 200 nm at best have been used for selective TPF imaging of specific fluorophores [15-17] and for multicolor MPM [18–21]. The implementation of a SC source based on a picosecond laser has also been reported, with additional optical amplifiers to demonstrate TPF bioimaging [22]. To our knowledge, no laser source meeting satisfactorily the three criteria previously identified has been revealed for MPM.

In this publication, we are demonstrating experimentally for the first time the ability of a low rate, simple and compact nanosecond SC source to generate multicolor multiphoton processes. This is illustrated by images of biological samples obtained from an unprecedented excitation bandwidth of 300 nm in the NIR. In the first part, the proof of principle of this new method is shown on resected samples of mouse muscle. Resulting images of TPF and SHG are compared with those obtained with a classical Ti : Sa excitation source. A further study on peak power levels involved is carried out to understand the similar image quality. In a second part, we are highlighting an adapted and comparable resolution in the micron scale to observe the expected interleaved structuration of the muscle. Finally, using nanosecond SC excitation, we demonstrate *in vivo* multicolor MPM by imaging tumor cells implanted in the brain of a mouse[1] simultaneously with the blood vessel network. In a simple way, the SC spectrum is shaped and adapted to the TPA spectra of both fluorophores used, covering the whole 300 nm SC bandwidth with their maxima separated by 150 nm, resulting in an optimized emission of TPF.

2. Experimental setup

The nanosecond SC laser results from the spectral broadening in a singlemode PCF of an amplified modulated laser diode centered at 1550 nm (1 ns, 10 µJ, 250 kHz). The PCF is 1 m long and has a Ge-doped silica core with a zero-dispersion wavelength close to 1400 nm. It is thus pumped in the anomalous dispersion regime, leading to SC generation from roughly 600 nm to 2400 nm. The resulting pulse duration of the SC source is 1 ns with 1 W of total average power. The spectrum is filtered between 700 nm and 1000 nm by using a set of high-pass and low-pass filters. The resulting average power of 120 mW is injected into an upright multiphoton microscope (BX61WI, Olympus, Japan) comprised of a scanning system, a water immersion microscope objective (XLPLN25XWMP, Olympus, Japan), two dichroic mirrors and two photomultiplier tubes (PMT) coupled with band-pass filters (575–630 nm; 390–420 nm for TPF and SHG channels respectively). A flip mirror allows the switch between excitations from the SC source to a femtosecond Ti : Sa laser (Chameleon Ultra II, Coherent, USA; 150 fs, 10 nm, 680–1080 nm, 80 MHz, 4 W). Figure 1a displays the experimental configuration.

Images can be obtained from either one or the other source without moving the microscope objective or the sample. The lateral and axial resolutions are respectively calculated at 0.4 µm and 1.3 µm considering an excitation wavelength of 810 nm.

[1] The use of animals has received the approval of the Ethical and Animal Care Committee (registration number: 15-2014-15). All animal cares and experimental procedures were conducted in conformity with the French Décret n° 2013–118 1st February 2013 NOR: AGRG1231951D in accordance with European Community guidelines (directive 2010/63/UE for the Care and Use of Laboratory Animals).

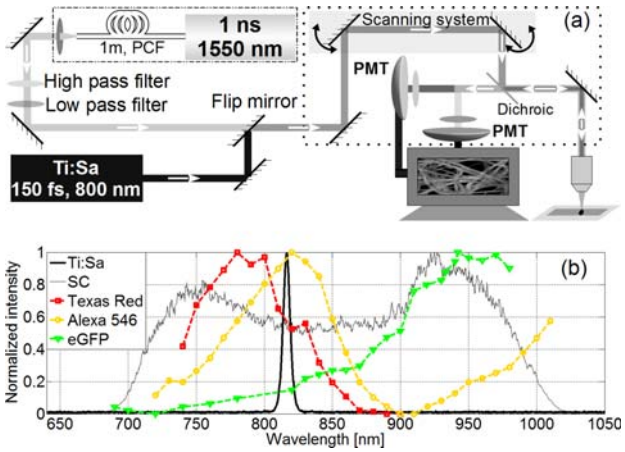

Figure 1 (**a**) Multiphoton imaging based on nanosecond SC or femtosecond Ti : Sa excitation. (**b**) Intensity spectra of nanosecond SC and femtosecond Ti : Sa sources. TPA spectra of Alexa Fluor® 546, eGFP and Texas Red® [25–27].

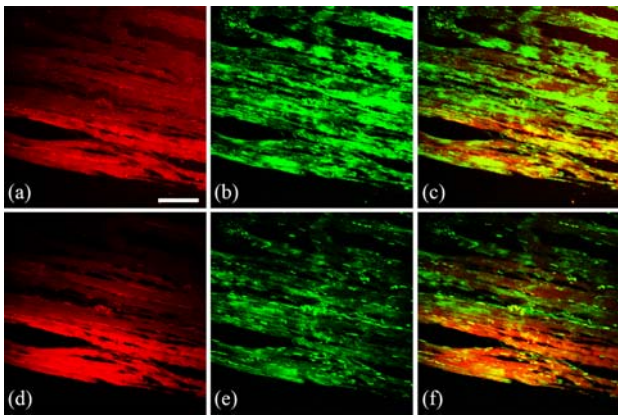

Figure 2 TPF and SHG images of mouse muscle (1024 × 1024 pixels, 100 µs/pixel). (**a**–**c**) Nanosecond SC excitation. (**d**–**f**) Femtosecond Ti : Sa excitation. (**a**, **d**) TPF. (**b**, **e**) SHG. (**c**, **f**) Superimposition of TPF (red) and SHG (green). Scale bar: 100 µm.

3. MPM with a nanosecond SC source

The sample is excised from the muscle of a mouse leg having a fibrous structure [23]. Each of the fibers is composed of discs of myosin and actin superimposed alternatively and perpendicularly to the axis of the fiber. Myosin organization is a non-centrosymmetric structure giving rise to SHG [24]. The presence of alpha-actinin, a cytoskeletal actin-binding protein, is labelled here by immunohistochemistry with a secondary antibody coupled to Alexa Fluor® 546. Consequently, the resulting specimen is ideal for both means of contrast: TPF of Alexa Fluor® 546 revealing the presence of alpha-actinin simultaneously with SHG from the myosin structure. The 4 µm cut is fixed on microscope glass slide. Figure 1b shows the intensity spectra of both laser sources measured at the microscope objective output, as well as the TPA spectra of Alexa Fluor® 546, eGFP and Texas Red® [25–27]. The Ti : Sa laser is centered at 810 nm, the maximum absorption of Alexa Fluor® 546.

Figure 2 displays 500 × 500 µm² images of mouse muscle, obtained from SC and Ti : Sa illuminations in the case of TPF, SHG and both combined with an identical color intensity (pixel dwell time 100 µs). As expected, the fibrous structure is revealed by the TPF (actin) and the SHG (myosin) whatever the excitation source, proving the ability of SC laser to provide satisfactory multiphoton images. The surface of the sample visualized with the SC source (Figure 2a) looks larger than with the Ti : Sa laser (Figure 2d), especially regarding TPF. Interestingly, TPF imaging under SC excitation is less sensitive to the random flatness of the sample surface resulting from the steps of excising, cutting and fixing. This difference results from the focal point spread in deepness due to the chromaticity of the objective with the 300 nm spectral bandwidth of the SC. A better axial resolution is logically obtained with the Ti : Sa laser. On the other hand, the SHG image obtained with the SC source (Figure 2b) is more contrasted because only 60 nm of the SC (780–840 nm range) contribute to the generation of the SH signal, which is detected between 390 nm and 420 nm.

Starting from this preliminary comparison, the available peak powers of both excitation sources are evaluated and compared. The PCF of the SC source is pumped in the anomalous dispersion regime, resulting in the spectral broadening towards longer wavelengths by means of modulation instability, soliton generation and soliton self-frequency shift [28]. In the normal dispersion domain, the spectral broadening is induced by four-wave mixing between solitons and dispersive waves [29], which in addition experience soliton collisions, cross-phase modulation and the Raman effect. After propagation in the PCF, with alternating temporal compression and stretching, the initial nanosecond monochromatic pump wave converts into a broadband nanosecond SC made of incoherent short pulses whose peak power can be from few tens of watts to few kilowatts [30]. The conversion efficiency from the 1550 nm pump laser (10 µJ, 10 kW, 2.5 W) to the used NIR range (700–1000 nm) is 5% giving rise to a highly structured nanosecond pulse with 500 nJ total energy and 0.5 kW peak power (considered on average over all the sub-pulses), corresponding to 125 mW of average power at 250 kHz. The resulting energy, peak power and average power delivered to the target are respectively 370 nJ, 370 W and 92 mW, versus 70 pJ, 460 W and 5.5 mW for the femtosecond Ti : Sa laser. The average peak power of the SC source is thus only 1.24 times lower than that of the Ti : Sa laser.

The experimental result shown in Figure 2 was finally expectable, considering the peak power being the main physical parameter of the excitation source responsible for the generation of multiphoton processes. Furthermore, no photo-damage was observed during the whole of experiments, whatever the laser source. Based on these observations, the nanosecond SC source is quite capable of generating TPF and SHG processes in the same way as the Ti : Sa laser does.

4. Comparison of the contrast

The different contributions of actin and myosin have been dissociated by zooming on a region of interest (ROI) at the micron scale shown in Figure 3. The micron scale organization of the muscle fibers is evident, regardless of the laser source chosen. The filaments of actin and myosin, revealed respectively by TPF and SHG, are organized in discs superimposed alternatively and perpendicularly to the axis of the fiber. The I discs (actin) and A discs (mainly myosin) are well identified. Here the low contrast of the TPF image obtained with the SC source (Figure 3a) is clearly visible, in comparison with the result achieved with the Ti : Sa laser (Figure 3d). The SHG image achieved with the SC source has high contrast and quality, as can be seen in Figure 3b.

TPF and SHG intensity profiles have been plotted along a line drawn in Figures 4a and 4c to quantify the image contrast, from a zoom of the area depicted in Figures 3c and f respectively. Figures 4b and d respectively show the intensity profiles, in arbitrary unit, for the SC and Ti : Sa lasers. The alternation between actin and myosin with antiphase profiles are clearly identified, highlighting the adapted lateral resolution of the multiphoton microscope regardless of the laser source with a periodicity of 2.2 μm, calculated over six periods. The calculated average contrast for TPF imaging under SC excitation (Figure 4a) is only 57.7%, in agreement with previous observations. For the TPF of Figure 4c and for the SHG of Figures 4a and c, the contrast is close to 100%. Finally, the double peak structure of the SHG signal, especially visible with SC excitation, can be attributed to the presence of H discs in the center of A discs. It is hypothesized that the decrease of SHG efficiency in this area is due to the particular molecular arrangement.

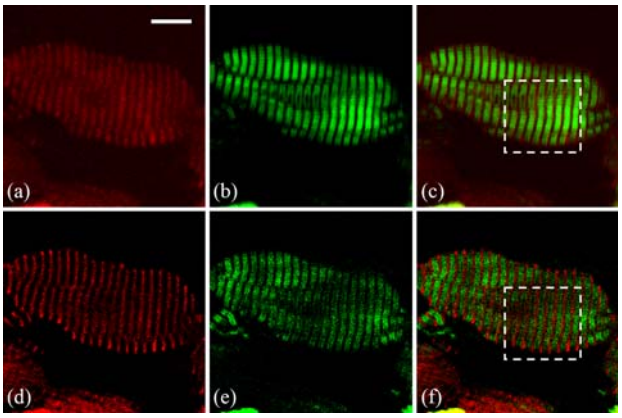

Figure 3 TPF and SHG images of mouse muscle at the micron scale (1024 × 1024 pixels, 100 μs/pixel). (**a**–**c**) Nanosecond SC excitation. (**d**–**f**). Femtosecond Ti : Sa excitation. (**a**, **d**) TPF. (**b**, **e**) SHG. (**c**, **f**) TPF (red) and SHG (green) superimposed. Dashes: area studied in Figure 4. Scale bar: 10 μm.

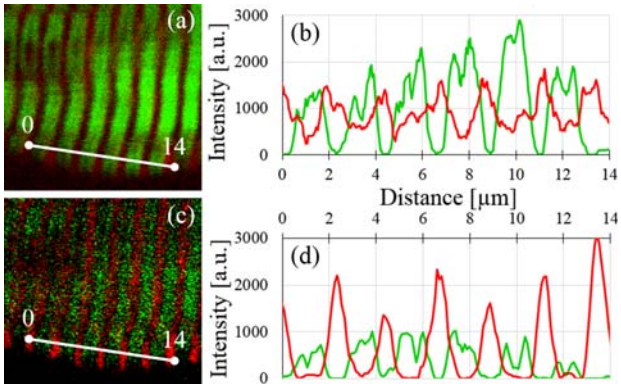

Figure 4 TPF (red) and SHG (green) intensity profiles plotted along the line drawn in (**a**) and (**c**) respectively under (**b**) nanosecond SC and (**d**) femtosecond Ti : Sa excitation.

The low contrast of TPF images (Figures 2a, 3a, 4a) can be improved by limiting the focal point spreading in deepness. This could be realized (i) by reducing the SC bandwidth to only tens of nanometers by means of filtering/shaping devices, or – preferably – (ii) by using an achromatic objective in the useful spectral range.

5. *In vivo* multicolor MPM

The SC source is used for MPM realized *in vivo* on the brain of a mouse anaesthetized with ketamine/xylazine, where glioma tumor cells (GL261) stably expressing eGFP were previously grafted thanks to the implementation of a cranial window as described in [31] and illustrated in Figure 5a. The organization of the cortical blood vessels evolve all around the tumor cells and is followed during several weeks thanks to a second fluorophore, Texas Red® conjugated Dextran (70 kD), injected in a tail vein. High pass and low pass filters (Figure 1a) are chosen in order to deliver an excitation spectrum having a

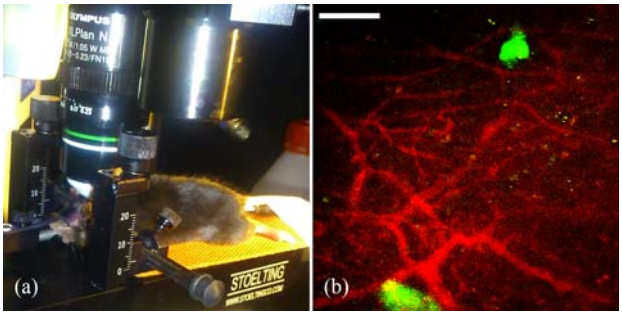

Figure 5 (**a**) Setup for *in vivo* imaging of mouse brain. (**b**) TPF image (512 × 512 pixels, 100 µs/pixel) of living mouse brain with grafted tumor cells expressing eGFP (green) and surrounded by a network of blood vessels labelled with Texas Red® conjugated Dextran (red). Scale bar: 100 µm.

shape fitting at best the sum and the maxima of the TPA spectra (Figure 1b). The TPA spectrum of Texas Red® is centered at 790 nm [27], versus 940 nm for the eGFP [26]. TPF is respectively detected in the ranges 580–700 nm and 490–540 nm. The optical power and pixel dwell time are the same as in part 3. Figure 5b shows the resulting image obtained in 26 s at 200 µm under the surface of the brain, five days after the grafting procedure. At that time, the blood vessels were not yet co-localized with tumor cells showing a low vascularization. No photo-damage was observed during the experiment.

The network of cortical blood vessels surrounding the xenografted tumor cells is clearly visible. The applicability of the SC laser source to TPF imaging is thus demonstrated in the presence of two fluorophores with TPA spectra separated by 150 nm and both covered by the 300 nm SC bandwidth. In the current structure of the microscope, the biological characterization of a sample is limited only by the two PMTs available. With more detectors, the characterization of a higher number of biological constituents or functions might be led. Faster imaging (∼1 fps) with the same 250 kHz SC source should be possible by reducing the pixel dwell time to 4 µs.

6. Conclusion and perspectives

We have shown experimentally for the first time that a nanosecond SC source with a low repetition rate is suitable for MPM and especially TPF and SHG imaging with a comparable image quality to that obtained with a classical Ti : Sa laser. *In vitro* and *in vivo* images of mouse muscle and brain were obtained by coupling a 250 kHz nanosecond SC laser coupled to a conventional multiphoton microscope. The use of this source is doubly justified and demonstrated. First, its broad spectrum allows the simultaneous excitation of several fluorophores with TPA spectra covering several hundreds of nm. Second, the technological simplicity of the laser with a low rate and nanosecond duration allows a new way of MPM with a source having a high compactness, high reliability, low cost and being maintenance-free.

Beyond these aspects, the interest of using such laser technology lies in its versatility, with available spectral bandwidth from the visible to the deep NIR. Along the same lines, higher-order multiphoton mechanisms might be accessible thanks to the longer wavelengths directly available from the SC source. Thus, extensive biological analysis could be conducted by means of a stable and turn-key microscopy system.

Acknowledgements This research was supported by the "Défi Imag'In" program from CNRS for the project "ARKENCIEL" and by the Région Limousin with the thematic call for projects. We especially thank Fabienne Baraige and Denise O'Connor for their technical help with the preparation of samples and mice.

References

[1] W. Denk, J. H. Strickler, and W. W. Webb, Science **248**, 4951 (1990).
[2] H. Segawa, Y. Kaji, P. Leproux, V. Couderc, T. Ozawa, T. Oshika, and H. Kano, J. Biophotonics **8**(9) 705–713 (2015).
[3] M. J. Booth and S. W. Hell, Journal of Microscopy **190**(3), 298–304 (1998).
[4] J. Bewersdorf and S. W. Hell, Journal of Microscopy **191**(1), 28–38 (1998).
[5] W. Denk, D. W. Piston, and W. W. Webb, Handbook of Biological Confocal Microscopy, Third Edition, 535–549 (2006).
[6] A. M. Larson, Nature Photonics **5**, DOI: 10.1038/nphoton.an.2010.2 (2011).
[7] J. Klein and J. D. Kafka, Nature Photonics **4**, 289 (2010).
[8] H. Segawa, M. Okuno, P. Leproux, V. Couderc, T. Ozawa, and H. Kano, Analytical Sciences **31** (2015).
[9] D. Vucinic and T. J. Sejnowski, PLos One **8** (2007).
[10] H. J. Koester, D. Baur, R. Uhl, and S. W. Hell, Biophysical Journal **77**, 2226–2236 (1999).
[11] M. Baumgart, T. Gottschall, J. Abreu-Afonso, A. Díez, T. Meyer, B. Dietzek, M. Rothhardt, J. Popp, J. Limpert, and A. Tünnermann, Optics Express **20**(19), 21010–21018 (2012).
[12] M. Baumgartl, M. Chemnitz, C. Jauregui, T. Meyer, B. Dietzek, J. Popp, J. Limpert, and A. Tünnermann, Optics Express **20**(4), 4484–4493 (2012).
[13] G. McConnell and E. Riis, Journal of Biomedical Optics **9**(5), 922–927 (2004).
[14] C. Lefort, M. Kalashyan, G. Ducourthial, T. Mansuryan, R. P. O'Connor, F. Louradour, Journal of Optical Society of America B **31**(10) 2317–2324 (2014).

[15] J. A. Palero, V. O. Boer, J. C. Vijverberg, and H. C. Gerritsen, Opt. Exp. **13**, 14 (2005).
[16] J. Tada, T. Kono, A. Suda, H. Mizuno, A. Miyawaki, K. Midorikawa, and F. Kannari, Applied Optics **46** (15), 3023–3030 (2007).
[17] X. Liu, J. Lægsgaard, U. Møller, H. Tu, S. A. Boppart, and D. Turchinovich, Optics Letters **37**(13), 2769–2771 (2012).
[18] K. Isobe, W. Watanabe, S. Matsunaga, T. Higashi, K. Fukui, and K. Itoh, Japanese Journal of Applied Physics **44**(2), 1–7 (2005).
[19] D. Li, W. Zheng, and J. Y. Qu, Opt. Lett. **34**, 2 (2009).
[20] W. Tao, H. Bao, and M. Gu, Journal of Biomedical Optics, **16**(5), 056010 (2011).
[21] X. Liang and L. Fu, IEEE Journal of Selected Topics in Quantum Electronics **20**(2), 6800108 (2014).
[22] H. Yokoyama, H. Tsubokawa, H. C. Guo, J. Shikata, K. Sato, K. Takashima, K. Kashiwagi, N. Saito, H. Taniguchi, and H. Ito, J. Biomed. Opt. **12**, 5 (2007).
[23] D. Jones, J. Round, and A. de Haan, Muscle from Molecules to Movement, Churchill Livingstone, Elsevier Limited, Oxford (2004).
[24] C. Odin, T. Guilbert, A. Alkilani, O. P. Boryskina, V. Fleury, and Y. Le Grand, Opt. Exp. **16**(20), 16151–16165 (2008).
[25] J. Mütze, V. Iyer, J. J. Macklin, J. Colonell, B. Karsh, Z. Petrasek, P. Schwille, L. L. Looger, L. D. Lavis, and T. D. Harris, Biophys. J. **102**, 934 (2012).
[26] Developmental Resource for Biophysical Imaging Opto-Electronics, http://www.drbio.cornell.edu/cross_sections.html, Cornell University.
[27] K. G. Heinze, A. Koltermann, and P. Schwille, PNAS **97**(19), 10377–10382 (2000).
[28] M. Andreana, A. Labruyère, A. Tonello, S. Wabnitz, P. Leproux, V. Couderc, C. Duterte, A. Cserteg, A. Bertrand, Y. Hernandez, D. Giannone, S. Hilaire, and G. Huss, Opt. Exp. **20**(10), 10750–10760 (2012).
[29] D. V. Skryabin and A. V. Yulin, Phys. Rev. E **72**, 016619 (2005).
[30] E. Räikkönen, G. Genty, O. Kimmelma, M. Kaivola, K. P. Hansen, and S. C. Buchter, Opt. Exp. **14**(17), 7914–7923 (2006).
[31] L. Sacconi, R. P. O'Connor, A. Jasaitis, A. Masi, M. Buffelli, and F. S. Pavone, J. Biomed. Opt. **12**, 050502 (2007).